

Multielectron excitations at the L edges in rare-earth ionic aqueous solutions

J. A. Solera, J. García, and M. G. Proietti

*Instituto de Ciencias de Materiales de Aragón, Consejo Superior de Investigaciones Científicas,
Universidad de Zaragoza, 50009 Zaragoza, Spain*

(Received 28 July 1994)

An extensive investigation of the extended x-ray-absorption fine structure (EXAFS) at the L edges of the rare-earth atoms of aqueous ionic solutions of La^{3+} , Ce^{3+} , Ce^{4+} , Nd^{3+} , Pr^{3+} , Eu^{3+} , Dy^{3+} , and Tm^{3+} at concentrations of 50, 100, and 200 mM, is presented. The presence of anomalous peaks, appearing in the range from 5 to 7 \AA^{-1} and superimposed to the main single-frequency oscillatory signal, has been explained as due to double-electron transitions $2p4d \rightarrow 5d^2$ in the case of L_3 and L_2 edges, and $2s4d \rightarrow 6p5d$ for the L_1 spectra. The energy of the double-excitation absorption edge increases as the atomic number of the element of the rare-earth series is increased and is in fair agreement with previous theoretical bound-to-bound calculations. The intensity of the anomalous feature decreases for increasing Z numbers, as expected from theory, but the intensity values, calculated from comparison with the main single-electron absorption line, are lower than those calculated by other authors and the double-excitation peak disappears in the Tm^{3+} spectrum. A structural analysis of the EXAFS spectra was also carried out with the twofold aim of characterizing rare-earth water solutions and quantifying the errors introduced in the structural parameters by the mixing of single- and double-electron phenomena. The results show the rare-earth ions are always surrounded by 12 water molecules and the rare-earth-O distance decreases with Z number, varying from 2.56 \AA for La^{3+} down to 2.32 \AA for Tm^{3+} . The presence of the anomalous peaks introduces small errors in the bond-length's determination, the effect being proportional to the magnitude of the double-excitation peak.

I. INTRODUCTION

During the last years one-electron theory, which neglects multielectron excitations, has dominated the field of x-ray-absorption spectroscopy. Nevertheless, the presence of multielectron transitions has already been observed in the x-ray-absorption coefficient of atoms.¹⁻⁶ The intensities characteristic of such a phenomenon are usually very low and the related anomalous features are difficult to observe in solid samples due to the presence of the quite structured oscillating extended x-ray-absorption fine-structure (EXAFS) background. The intensity associated with this kind of excitations is comparable with the amplitude of the EXAFS oscillation only in a few systems, allowing an unambiguous identification of their energy position and shape. As a consequence, multielectron transitions have been easily identified only in a small number of cases, mainly in disordered systems, and only in a few crystalline samples.⁷⁻¹³

We already observed an anomalous feature superimposed to the EXAFS oscillation in some intermetallic alloys as LaRu_2 , CeFe_2 , and CeRu_2 after hydridation.^{8,11-13} The identification of the anomalous peak as a multielectron excitation, was made possible by the effect of the hydridation process which induces a large disorder around the rare-earth atom smearing out the EXAFS oscillation. A little structure appears in all the hydridated samples at the L_3 EXAFS spectra independent of the hydridation degree. We attributed this feature to an intratomic electron transition involving two electrons, $2p$ and $4d$, giving a final state with two holes $2p4d$ and two parti-

cles $(5d)^2$.¹² Recently, anomalous features in the L_3 EXAFS spectra of cerium nitrate, LaNi_2 , and rare-earth-doped silica gel compounds have been detected at energy values coinciding with previous findings.^{14,15} These experiments clarify that the multielectron excitations appearing in rare-earth L_3 spectra are independent of the atomic chemical state and have an atomic origin. The presence of double-electron excitations at the rare-earth L_1 edge is more difficult to individuate. Only few experiments have been performed at the L_1 edge because, due to the low L_1 cross section and the consequently worse signal-to-noise ratio, the measures are more complicated and the detection of anomalous features is even less clear. The existence of the double-electron excitations at the L_1 edge has been reported in Ref. 14 but the quite large noise makes the result unclear.

Theoretical calculations based on a many-body perturbation method have been performed for the $LN_{4,5}$ excitations of the sixth-row elements. The energy position and cross section relative to the L main lines have been reported for the whole series. Transitions $2p4d \rightarrow 5d^2$ are shown to determine the $L_{2,3}$ resonance, while the process $2s4d \rightarrow 6p5d$ dominates at the L_1 edge.^{15,16}

The main goal of this work is to verify the atomic character of the detected features and to investigate its trend in the rare-earth series. The ideal experiment would be to study these elements in the gas phase, but, due to the low rare-earth vapor pressure, the spectra are very noisy, making the detection of small anomalies practically impossible. Some experiments in the gas phase were performed indeed, by the HasyLab group¹⁷ but only the x-

ray-absorption near-edge structure (XANES) region was measured. As we have pointed out before, the use of solid compounds makes it also difficult to distinguish anomalous structures from the single-electron EXAFS oscillations. They have been detected in a few cases by comparing the L_3 and L_1 spectra of rare-earth oxides.¹⁴

These technical problems could be overcome by the use of liquid samples. It is well known that the EXAFS spectrum of diluted ionic solutions is composed by a unique oscillation frequency coming from the scattering with the water first coordination shell.¹⁸ In this case the detection of a small feature, superimposed to an oscillation with a much longer period, is much more direct and the comparison of the L_1 and L_3 spectra would make it even easier.

Only a few structural experiments have been performed, to our knowledge, on rare-earth transition metals in water solutions.^{19–21} Something appears in the Ce^{3+} and Ce^{4+} spectra^{22–24} at about 130 KeV above the L_3 edge but the authors filter the small feature out.

In the present paper, we report a systematic experimental EXAFS study of the rare-earth ions in water solution. X-ray-absorption spectra at the L_1 , L_2 , and L_3 edges of the rare-earth ions La^{3+} , Ce^{4+} , Ce^{3+} , Pr^{3+} , Nd^{3+} , Eu^{3+} , Dy^{3+} , and Tm^{3+} at 50, 100, and 200 mM have been recorded. The identification of anomalous structures was performed by comparing the EXAFS signals of the different solutions and by comparison of L_3 , L_2 , and L_1 spectra of the same rare earth. We will show that a multielectron excitation is present at the L_3 and L_2 edges in almost all the elements of the series and that its intensity decreases with the atomic number disappearing for Tm. The L_1 spectra also present an anomalous behavior but it is more difficult to isolate the anomaly from the underlying EXAFS background.

A systematic study of the coordination of rare earths in a water solution has also been performed. We have determined the coordination geometry finding that rare-earth ions are always coordinated with 12 water molecules independent of the rare-earth concentration, at least in the range of concentration studied. The interatomic distances have also been determined and they decrease, as expected, with the rare-earth atomic number. A careful analysis has been performed in order to quantify the possible errors introduced by the presence of the many-body anomaly.

II. EXPERIMENTAL DETAILS

The aqueous solutions were prepared by diluting rare-earth chlorides in de-ionized water at concentrations of 0.05, 0.1, and 0.2 M. Ce^{4+} was diluted in a previously acidified solution of $pH=1$. Tm_2O_3 reference samples were prepared by dispersion of the proper amount of the pure oxides in boric acid and pressing the powder in pellets.

The experiments were carried out at the Synchrotron Radiation Source of the Daresbury Laboratory. The storage ring was operating at 2 GeV and the average current stored was about 200 mA. The absorption spectra at the L edges of rare earths were recorded at Station

7.1. The beamline was equipped with a Si(111) double-crystal monochromator and 50% of harmonic rejection achieved by slightly detuning the two crystals from the parallel alignment. The absorption experiments were performed at room temperature in the transmission mode using mylar cells with thickness ranging from 0.5 to 4 mm. Different thicknesses were used depending on the rare-earth element and on the edge (the L_1 edges were normally measured in a cell whose thickness was twice those used to measure the L_3 spectra). The incident and transmitted intensities through the sample were recorded by two ionization chambers filled with a mixture of He and Ar that was optimized for each edge. Two typical absorption spectra are shown in Fig. 1 for the L_3 edge of Tm and La. One can observe how the white lines are sharp and very intense with respect to the absorption jump, ensuring the absence of higher harmonics, that would artificially lower the absorption, as well as the good energy resolution achieved, that is estimated to be about 2 eV.

The experimental EXAFS spectra were extracted from the raw spectra by following standard methods.²⁵ The background from previous edges (μ_B) was removed by pre-edge polynomial fitting and the atomic absorption coefficient (μ_0) was determined by a cubic spline approximation to obtain the EXAFS oscillating signal defined as $\chi(k)=[\mu(k)-\mu_B(k)-\mu_0(k)]/\mu_0(k)$, where the photoelectron vector k is given by $k=(2m/\hbar^2)\sqrt{(E-E_0)}$. The energy origin E_0 , corresponding to the absorption threshold, was defined as the inflection point of the ab-

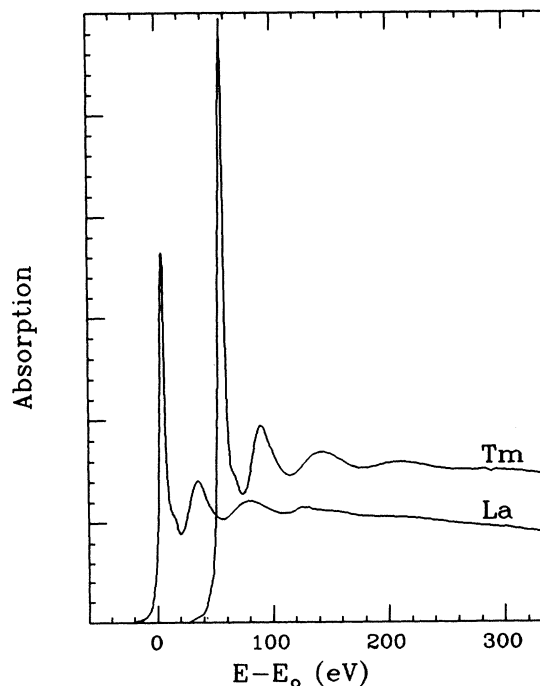


FIG. 1. Background subtracted x-ray absorption L_3 spectra of La^{3+} and Tm^{3+} water solutions. Note the intensity and sharpness of the white lines. The Tm spectrum has been shifted by 50 eV for sake of clarity.

sorption edge. The EXAFS signals, $\chi(k)$, were Fourier transformed by using in all the cases the same Gaussian window with the same k limits ($k_{\min}=2.5 \text{ \AA}^{-1}$, $k_{\max}=9 \text{ \AA}^{-1}$). The modulus of the Fourier transforms (FT) shown in the following are not corrected for the central atom phase shifts so that the peaks are shifted with respect to the true R values.

III. RESULTS AND DISCUSSION

A. Identification of the multielectron excitation

The L_3 , L_2 , and L_1 EXAFS spectra for the same rare-earth atom at the three concentrations studied are very similar showing that the rare-earth coordination as well as the anomalous structures appearing in the spectra, do not change for concentrations varying from 0.05 to 0.2 M. The L_1 , L_2 , and L_3 spectra of Pr^{3+} at concentrations of 0.05 and 0.2 M are compared in Fig. 2.

The L_3 EXAFS spectra of different rare-earth ionic aqueous solutions ($R=\text{La}^{3+}$, Ce^{3+} , Pr^{3+} , Nd^{3+} , Eu^{3+} , Dy^{3+} , Tm^{3+}) are reported in Fig. 3. They are characterized by the same oscillating behavior which reveals the existence of a first shell local order around the rare-earth site. The EXAFS signal is formed by a near single-frequency oscillation indicating that only an ordered coordination shell is seen from the rare-earth site. A small feature in the range from 5 to 7 \AA^{-1} appears super-

imposed to the main oscillation. Its intensity decreases with the rare-earth atomic number and it disappears for the Tm spectrum that is the last of the series.

The same Tm spectrum can be used, on the basis of the following considerations, to separate the anomalous features appearing in the lower atomic number spectra, from the EXAFS background. The difference we observe among the single-frequency EXAFS signals of the different R solutions is associated with a change of frequency due both to the small change of the R -O bond length across the series and to the different central-atom phase shift. Therefore, considering that the differences of central-atom phase shifts among the various element of the R series are quite small and, as a first approximation, nearly linear in k , we can superimpose all the spectra of the series to the Tm spectrum through a proper k rescaling:

$$k_{\text{rescaled}} = f(R) \cdot k_{\text{experimental}},$$

being $f(\text{La})=0.9268$, $f(\text{Ce})=0.9321$, $f(\text{Pr})=0.9333$, $f(\text{Nd})=0.9495$, $f(\text{Eu})=0.9708$, $f(\text{Dy})=0.9876$. The constant values $f(R)$ has been obtained by best fitting of the Tm spectrum with the spectra of the other elements of the series.

The result of this simple analysis is shown in Fig. 3. We can observe how the rescaled Tm spectra fairly coincide with the EXAFS oscillations of the whole series indicating that coordination around the rare-earth ion is the same for all the samples and that the anomalous feature

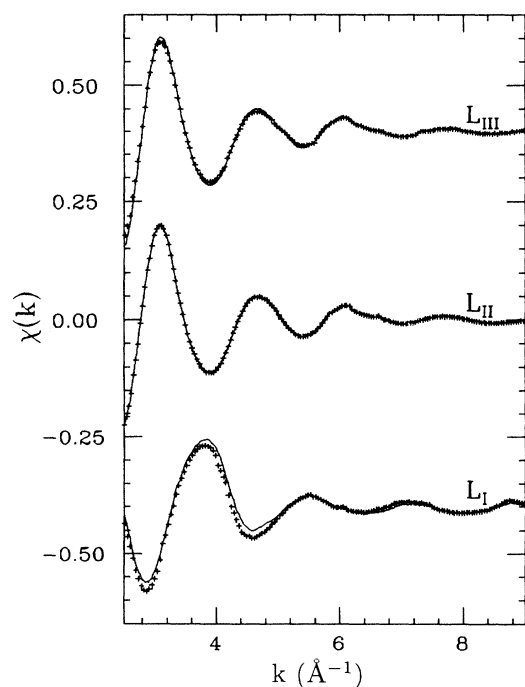


FIG. 2. Comparison of the L_3 , L_2 , and L_1 EXAFS spectra of Pr^{3+} water solutions at 0.05 M (continuous line) and 0.2 M (dotted line) concentrations. The zero of the vertical axis refers to the L_2 spectrum, the other spectra are shifted upwards and downwards for sake of clarity.

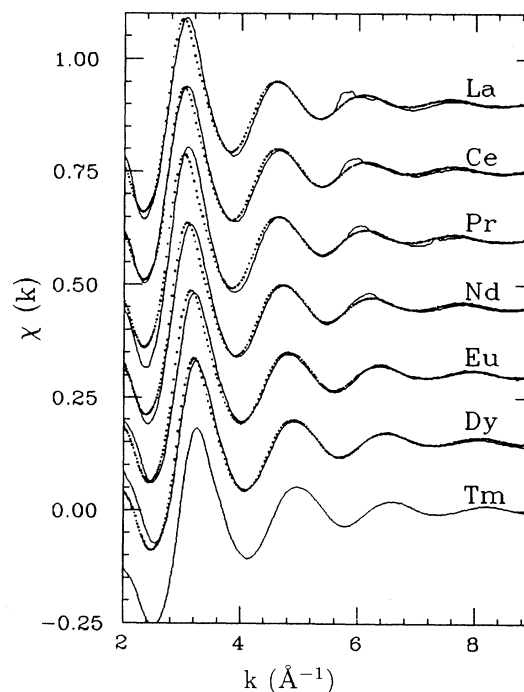


FIG. 3. Experimental L_3 rare-earth EXAFS spectra of La^{3+} , Ce^{3+} , Pr^{3+} , Nd^{3+} , Eu^{3+} , Dy^{3+} , and Tm^{3+} aqueous solutions (solid line) and Tm^{3+} scaled spectra (see text) (dotted line). The zero of the vertical axis refers to spectrum of Tm, the other spectra are shifted upwards for sake of clarity.

can be isolated in a simple way from the underlying EXAFS signal. The detail of the region from 5 to 7 \AA^{-1} , in which the multielectron excitation appears, is shown in Fig. 4. As can be observed, the anomalous feature intensity decreases as the atomic number Z increases until no appreciable difference is observed between Dy and Tm. The fact that the position in energy of these structures varies as a function of the rare-earth atomic number whereas the EXAFS remains unchanged after rescaling, strongly suggests that they are due to many-body intra-atomic processes.

A more accurate measure of La, restricted to the region of the multielectron excitations is shown in Fig. 5. The La L_3 spectrum was recorded with a step in energy of 0.25 eV and a fine structure is clearly observed above the onset of the anomaly. The two first peaks above the double-excitation edge could be related to relativistic splitting of the $2p, 4d \rightarrow 5d, 5d$ transition, the shift in energy of about 4 eV in agreement with the calculated value from Ref. 15. A few further structures are observed too on the high-energy side, recalling a fine structure, i.e., related to chemical and/or structural effects. A similar behavior is observed also in the other elements of the series although it is more and more broadened for increasing Z numbers. It is worth remarking that the shape of the same kind of anomaly, observed in a previous work on R hydrides at the L_3 edge of La,¹² was appreciably different pointing to the presence of some chemical and/or structural effect and the subject is a

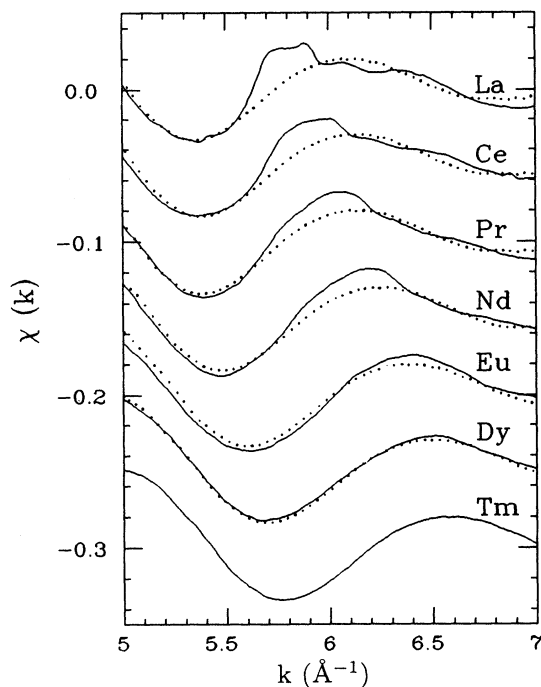


FIG. 4. Detail of the L_3 EXAFS spectra of rare-earth aqueous solutions (solid line) and their corresponding scaled Tm^{3+} spectra (dotted line) in the k ranges 5–7 \AA^{-1} . The zero of the vertical axis refers to the La spectrum, the other curves are shifted downwards for sake of clarity.

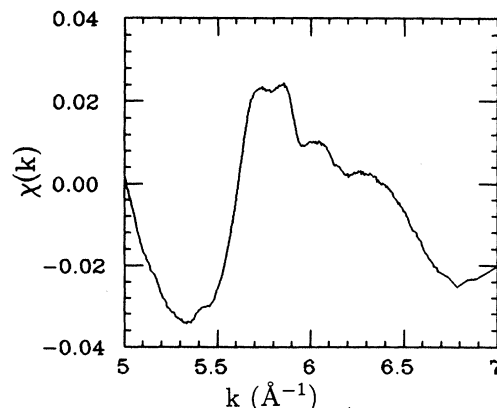


FIG. 5. Detailed measurement of the anomaly at the La L_3 edge. The spectrum was taken with a step in energy $\Delta E = 0.25$ eV.

matter for further study.

The comparison between L_2 and L_3 spectra for the whole series is shown in Fig. 6. The double-electron excitation appears, as expected, in the L_2 spectra too, and the L_3 and L_2 spectra are very similar to each other. The Ce^{3+} spectrum is the only exception showing a different intensity of the anomalous peak.

In order to clarify that the anomalies observed in the L_3 and L_2 spectra do not derive from scattering events

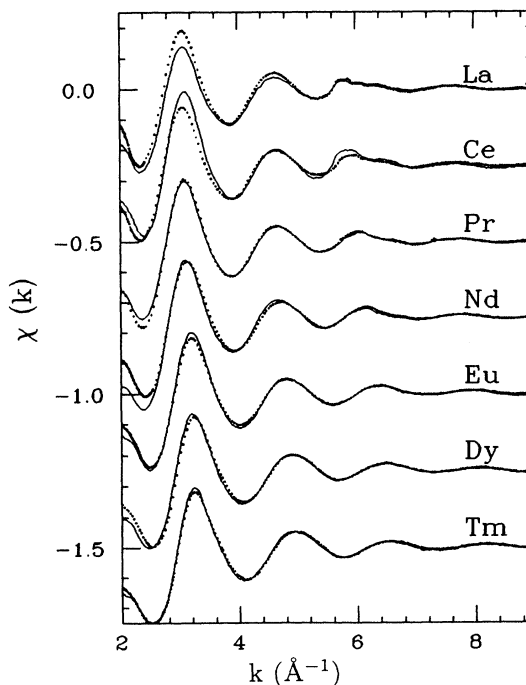


FIG. 6. Comparison of the signal corresponding to the absorption at the L_3 (solid line) and L_2 (dotted line) edges of rare-earth aqueous solutions. The zero of the vertical axis refers to the La spectrum, the other curves are shifted downwards for sake of clarity.

we have also compared the L_3 and the L_1 spectra. It is well known that the L_3 and L_1 EXAFS present the same oscillating behavior, except for a π shift and the different central-atom phase shifts related to the different kind of core electronic transition. On the contrary, features not associated to single-electron excitation events would not show the same behavior. As shown in Ref. 26, the L_1 spectrum cannot be reproduced from the correspondent L_3 edge by a simple π change (the so-called " π approach") and it is necessary to also take into account the different central-atom phase shifts for excitations from $2p$ ($l=1$) and $2s$ ($l=0$) core levels. Adopting the approximation that the difference between the L_3 and L_1 central-atom phase shifts, i.e., $\Delta\delta = \phi^{l=2}(k) - \phi^{l=1}(k)$, is linear in k , we can generate the L_3 signal from the L_1 spectrum multiplying it by -1 (π phase shift) and operating a linear k rescaling to take into account $\Delta\delta$. The procedure is just the same as that used for the comparison and k rescaling of the Tm L_3 spectrum to fit it to the other spectra of the L_3 series. This time the rescaling is related to the phase shift change due to the different kind of edge of the same material, while in the former case it was due both to the change of bond length and phase shifts of the different atomic species. The L_3 EXAFS spectra are compared with the rescaled and inverted L_1 signals of the same element in Fig. 7. A satisfactory overall agreement is obtained for the whole L_3/L_1 series and, at the same time, the well observable anomaly appearing in the L_3

signals is still evident in the same k region confirming that its origin is not related to single-electron scattering events.

A careful analysis of the L_1 spectra has been also carried out since the presence of double-excitation features cannot be excluded from the above L_1 - L_3 comparison. We performed therefore the same analysis employed for the L_3 edges on the L_1 spectra, i.e., we used the last element of the series whose anomaly is so weak that it is no longer observed, to fit the EXAFS background of the others. The signal used in this case as reference and rescaled to fit the others, is that of Dy instead of that of Tm. The intensity of the anomaly is indeed lower than in the L_3 series and the signal-to-noise ratio of the spectra is also worse, the L_1 cross section being considerably lower than the L_3 one. Therefore the Dy signal was considered more suitable than Tm showing a better signal-to-noise ratio and the anomaly no longer being detected. We used the same kind of linear k rescaling applied to the Tm signal but fitting La, Ce, Pr, Nd, and Eu with Dy. Very broadened anomalous features appear in the range $5-7 \text{ \AA}^{-1}$ in analogy with those detected in the correspondent L_3 spectra of the same elements and they are shown as shaded areas in Fig. 8 where the L_1 -edge EXAFS spectra of La, Ce, Pr, Nd, and Eu are compared with the k -scaled Dy spectrum. In this case, the anomalous features seem to be located at the oscillation minima and, due also to the larger noise/signal ratio of the L_1 spectra, it is more complicated to isolate the anomalies from the EXAFS background. However, the shaded areas shown in Fig. 8

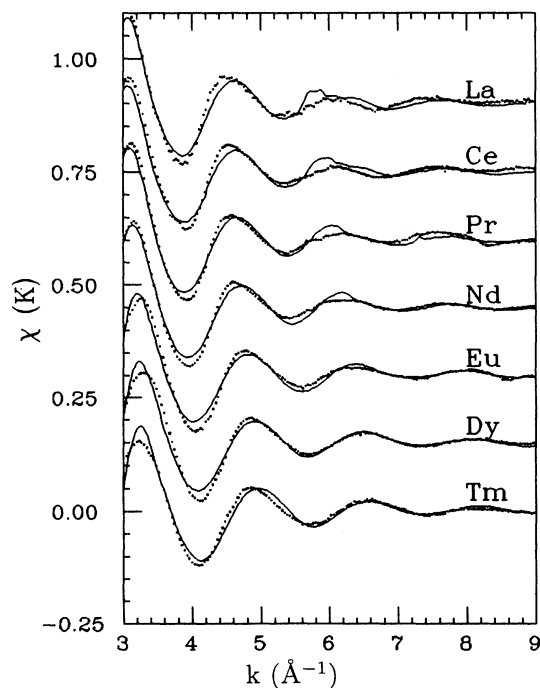


FIG. 7. Comparison of the signals corresponding to the absorption at the L_3 edge of rare-earth aqueous solutions (solid line) and those obtained starting from the L_1 signal (dotted line) using the method described in the text. The zero of the vertical axis refers to the Tm spectra, the other curves are shifted upwards for sake of clarity.

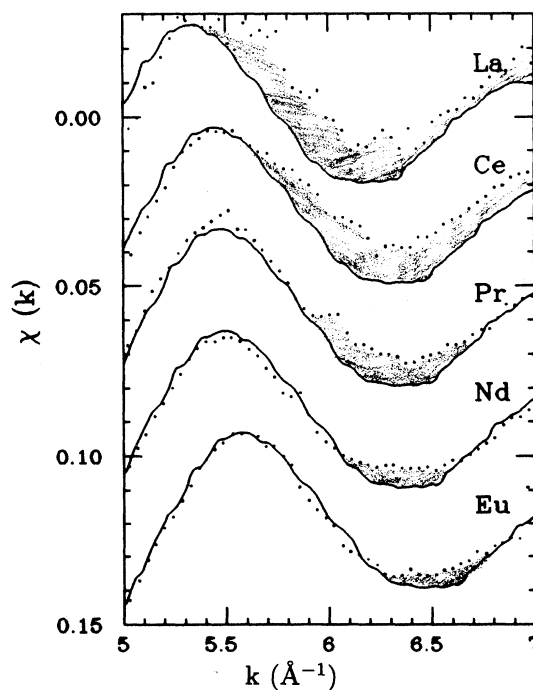


FIG. 8. L_1 EXAFS spectra of the rare-earth aqueous solutions (solid line) and their corresponding scaled Dy^{3+} spectra (dotted line) in the k range between $5-7 \text{ \AA}^{-1}$. The zero of the vertical axis refers to the La spectrum, the other curves are shifted downwards for sake of clarity.

can be related to an anomalous feature since they appear in the energy region previewed by theory¹⁶ and, as occurs for the L_3 spectra, they decrease in intensity and shift to higher energy for increasing rare-earth atomic numbers. A similar feature has been observed in rare-earth-doped gel materials and associated to a double electronic transition from a $2s4d \rightarrow 6p5d$ transition.¹⁵

In order to assign the structures observed to a specific many-body transition we have compared our results with the previous cross section theoretical calculations.^{15,16} To calculate the intensity of the experimental anomalous features relative to the main $2p \rightarrow 5d$ bound transition, we have applied the following procedure that is illustrated in Fig. 9 for the Dy^{3+} L_3 edge. The experimental near-edge region was deconvoluted as sum of an arctg function, representing the transition to the continuum, with a Lorentzian curve which represents the white line, i.e., the transition from the $2p$ to the $5d$ bound state. The area of the Lorentzian peak gives a measure of the transition cross section and the intensity of the anomalous feature could be estimated by integrating the difference between the experimental spectrum and the Tm^{3+} rescaled signal. This estimation is of course qualitative, due also to the structured nature of the double-excitation feature, and is reported to give a qualitative comparison between experiment and the theoretical calculations of the bound-state double-electron transitions. The intensity ratios between the main transition and the two-electron transition have been calculated for the whole series and are reported in Table I together with the theoretical values from Ref. 16.

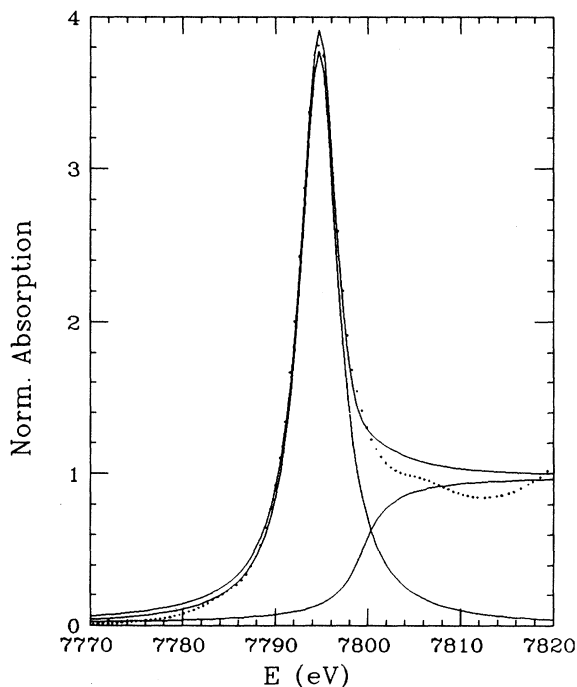


FIG. 9. Deconvolution of the L_3 -edge absorption spectrum of Dy^{3+} water solution as sum of an arctg function, representing the transition to the continuum, and a Lorentzian curve representing the transition to the bound $5d$ state.

TABLE I. $2p4d \rightarrow 5d^2$ double electron transition intensities and excitation energies of the rare-earth series at the L_3 edge of rare earths. Theoretical data have been taken from Refs. 14 and 15. R is the rare earth; $\sigma_D/\sigma_S(\text{exp})$ is the ratio between experimental cross section strengths of the double excitation and of the white line in % calculated as described in the text; $\sigma_D/\sigma_S(\text{teo})$ is the ratio between theoretical values. ΔE is the energy of the double excitation relative to the single-hole state.

R	$\sigma_D/\sigma_S(\text{exp})$ %	$\sigma_D/\sigma_S(\text{teo})$ %	$\Delta E(\text{exp})$ eV	$\Delta E(\text{teo})$ eV
La	1.2 ± 0.2	2.16	125 ± 5	123
Ce	0.74 ± 0.2	1.66	129 ± 5	122
Pr	1.1 ± 0.2	1.40	127 ± 5	128
Nd	0.7 ± 0.2	1.20	135 ± 5	134
Eu	0.5 ± 0.2	0.80	156 ± 5	152
Dy	0.2 ± 0.2	0.56	162 ± 5	170

The experimental energy shift of the $2p,4d \rightarrow 5d^2$ double-electron transition with respect to the main $2p \rightarrow 5d$ transition is in fair agreement with the theoretical values. It has been estimated as the difference between the energy of the anomaly maximum and the energy of the absorption threshold (E_0), a quite large error is given on the estimated values due to the structured and/or broadened nature of the anomalous features. A qualitative agreement is instead obtained for the transition cross sections. The experimental intensity ratios values, σ_d/σ_s , are in general lower than the calculated ones and show a faster decrease with the atomic number (see Table I).

Regarding the L_1 edges, it is more difficult to evaluate the positions in energy of the double-electron transitions, since they are very broadened and only a qualitative agreement with the theoretical data can be established. As far as the intensity ratios are concerned, the calculations reported in Ref. 15 show that they are similar to the correspondent values for the L_3 spectra but, on an experimental point of view, it is hard to give an estimation of the double-excitation strength with respect to the one-electron transition. In the case of the L_1 edge indeed, the one-electron excitation takes place through a $2s \rightarrow 6p$ transition and, the $6p$ state extended to the continuum, it is impossible to evaluate the transition strength as for the bound-to-bound transition responsible for the L_3 white line. We could have an idea, on a qualitative point of view, of the experimental intensity ratio of the double-to-single transition at the L_1 edge by comparing the shaded region area shown in Fig. 8 with the L_1 experimental cross section, taken as the absorption edge jump, and making the same comparison for the L_3 edge. We observe that the L_1 and L_3 double-electron transition intensities show similar values of the ratio with the correspondent L_1 and L_3 one-electron transitions, agreeing in this sense with the similar σ_d/σ_s ratios obtained by the theory.

B. Structural analysis

The modulus of the Fourier transforms (FT) of the k -weighted experimental L_3 EXAFS spectra, performed in

the k interval $2.5-9 \text{ \AA}^{-1}$ and using a Gaussian window, are reported in Fig. 10. A main peak corresponding to the first coordination water shell is observed, some other smaller peaks appear at higher and lower distances. The amplitude of these peaks, mainly that observed at low R values, are indirect evidences of the presence of multielectron excitations as already suggested by other authors.²⁷ The intensity of these peaks decreases indeed, with the atomic number according to the decreasing intensity of the anomalous features present in the EXAFS signals.

The presence of the multielectron excitations makes, therefore, the EXAFS analysis particularly delicate. The use of model compounds is not possible for the low- Z rare earths, since anomalous structures are present in the models as well, distorting phases and amplitudes. Things are easier for the R with a higher- Z number due to the decreasing intensity of the anomalous features. Theoretical phases and amplitudes have been used therefore to carry out the structural analysis of the spectra and a check on their reliability was done on Tm_2O_3 .

The theoretical EXAFS signals have been generated using the FEFF3.11 code²⁸ and tested for the Tm-O pair through the analysis of the first coordination shell of Tm_2O_3 oxide. The theoretical EXAFS spectrum at the rare-earth L_3 edge was calculated for a cluster of eight oxygen atoms located at 2.3 \AA from the R absorber atom. The Fourier-filtered EXAFS spectra were analyzed by least-squares minimization of the difference between experimental and theoretical data. The fit parameters,

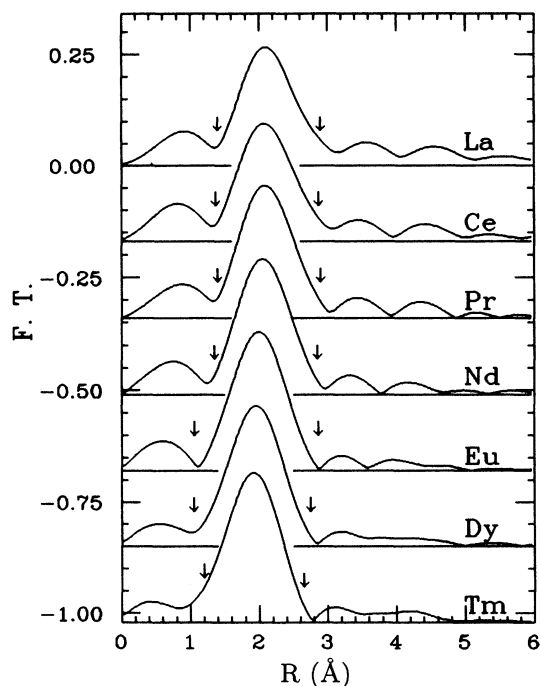


FIG. 10. Fourier transform modulus of the L_3 EXAFS spectra of the rare-earth aqueous solutions. The zero of the vertical axis refers to the La spectrum, the other curves are shifted downwards for sake of clarity.

TABLE II. Best-fit values obtained for coordination numbers (N), interatomic distances (d), and Debye-Waller factors (σ^2), of the first oxygen shell of Tm_2O_3 compared with the crystallographic data. The subscript "cryst" correspond to crystallographic data taken from Refs. 29 and 30. The errors on the fit parameters have been estimated according to Ref. 31 and are (see also text): $\Delta N/N \cong 10\%$, $\Delta R = \pm 0.01 \text{ \AA}$, $\Delta \sigma^2 = 0.003 \text{ \AA}^2$.

	n	d (\AA)	σ^2 (\AA^2)	N_{cryst}	$d_{(\text{cryst})}$
Tm_2O_3	6	2.23	0.0066	6	2.231

iterated until least-squares minimization was achieved, were coordination number N , distance d , and Debye-Waller factor σ^2 . The errors on the fit parameters were evaluated by changing each variable, while refining the others, until the residual at minimum was doubled.³¹

The EXAFS of Tm_2O_3 was Fourier transformed in the range $2.5-9 \text{ \AA}^{-1}$ and the first shell EXAFS contribution obtained by Fourier filtering in the range $0.85-2.5 \text{ \AA}$. The comparison between the experimental filtered spectrum and best fit is reported in Fig. 11(a). The best-fit results are reported in Table II and compared with the crystallographic data.^{29,30} The relative error on coordi-

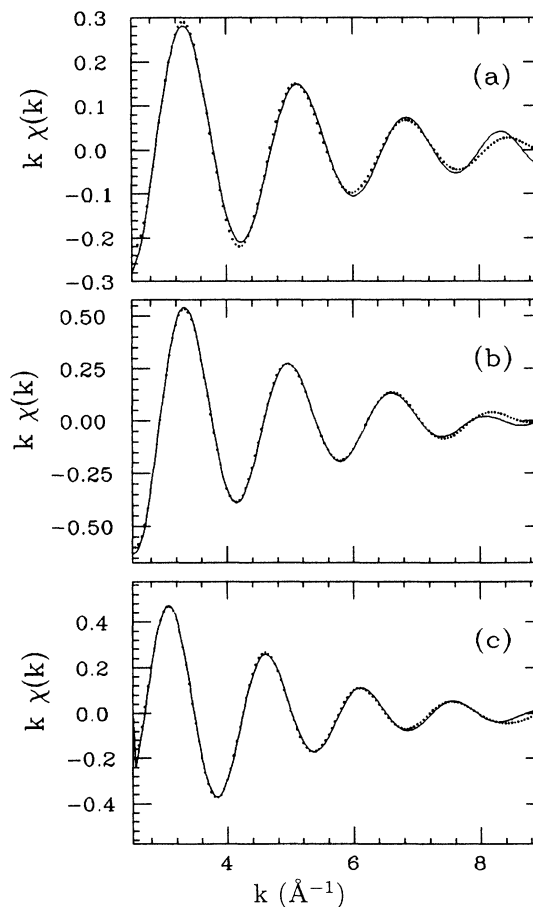


FIG. 11. k -weighted Fourier-filtered EXAFS of the first shell (continuous line) and best fit (dotted line) of the L_3 edge of Tm_2O_3 (a), Tm^{3+} (b), and La^{3+} (c) water solution. The best fit for La was performed on the Tm^{3+} k -rescaled signal.

nation numbers is of about 10%. The errors on Debye-Waller factors and bond lengths are of about 0.003 \AA^2 and 0.01 \AA , respectively. The excellent agreement between the crystallographic and EXAFS data makes us confident of the reliability of the theoretical phase shifts and amplitudes generated by the same code for the rest of the *R* series.

In order to establish the influence of the anomalous peak on the EXAFS analysis and consequently, on the error in the structural parameters and, on the other hand to determine the coordination sphere of water solutions of rare-earth ions, we have performed the spectra analysis following two different procedures. First, the experimental spectra were Fourier filtered in the range indicated by the arrows in Fig. 10 and a best fit performed by least-squares minimization of the difference between experimental and theoretical data. The second method consists of using the rescaled Tm^{3+} signals, shown in Fig. 3, as experimental EXAFS spectra of the different samples. They were able to reproduce well the double-excitation-free background of the other components of the series, removing the anomalous features from the spectra. The best fit was then performed as above but on signals in which the anomaly was in some way filtered out. The comparison with the results obtained using the former procedure can give an idea of the errors induced by the presence of the double-excitation features. The structural parameters obtained in the two cases are reported in Table III, the fit parameters were again coordination number *N*, distance *d*, and Debye-Waller factor σ^2 . The errors have been estimated as mentioned above and the values found are equal for both analysis procedures and similar to those found for the oxide (see table). For illustration, the best fits of Tm^{3+} and La^{3+} solutions are compared with the experiment in Figs. 11(b) and 11(c), respectively. The fit reported for La is that performed, following the second method, on the correspondent *k*-rescaled Tm signal.

The coordination numbers, corresponding to the first shell contribution of the *R*-O pairs, are shown to be the same and equal to 12 for all the samples, indicating a cubooctahedral symmetry of the water molecules around the *R* atom. The *R*-O bond length decreases for increasing atomic numbers as expected from the decreasing ion-

TABLE III. Structural parameters obtained from the L_3 EXAFS spectra of the rare-earth ions in water solution: coordination numbers (*N*), interatomic distances (*R*), and Debye-Waller factors (σ^2). Subscript 1 indicates parameters obtained by best fit of the experimental spectra including the anomaly of the double electron excitation. Subscript 2 refers to the data obtained after removing the anomalous structure (see text). The errors on the fit parameters are $\Delta N/N \cong 10\%$, $\Delta R = \pm 0.01 \text{ \AA}$, $\Delta \sigma^2 = 0.003 \text{ \AA}^2$, for the whole set of samples.

	R	La	Ce	Pr	Nd	Eu	Dy	Tm
<i>N</i>		12	12	12	12	12	12	12
R_1 (Å)		2.58	2.55	2.54	2.49	2.41	2.37	2.32
R_2 (Å)		2.56	2.53	2.52	2.48	2.41		
σ_1^2 (Å ²)		0.008	0.0087	0.0065	0.0067	0.0075	0.0077	0.0075
σ_2^2 (Å ²)		0.0087	0.0084	0.0082	0.0082	0.0074		

ic radius. A small difference of interatomic distances is observed for La, Ce, and Pr for the two different methods and can be directly related to the presence of the anomaly that is more important, as we know, for the low-*Z* number *R* atoms.

We would also like to mention that Ce^{4+} water solutions have been measured as well but a similar kind of analysis is not possible for this system. It is well known indeed that the XANES spectrum of Ce^{4+} is characterized by a double peak originated by the existence of two excitation channels coming from the two ground-state electronic configurations (f^0 and f^1).^{32,33} It has been suggested that these two channels are extended to the EXAFS region in such a way that two different EXAFS contributions, coming from the two configurations, would be mixed in the overall spectrum.³³ Our data show that the amplitude of the EXAFS spectra is much lower than those observed either for Ce^{3+} and for the rest of the series suggesting a possible out-of-phase superposition of different contributions. A detailed analysis of the Ce^{4+} spectrum and its possible deconvolution in two different channels is the object of a future work and is a little outside of the aim of this paper. Nevertheless, we would like to show that an anomalous structure has been observed also in the L_3 and L_2 spectra of Ce^{4+} located at the same energy as in the Ce^{3+} spectra. The Ce^{4+} L_3 and L_2 EXAFS spectra are compared with the L_3 spectrum of Ce^{3+} in Fig. 12. The presence of the anomaly demonstrates again that its presence is independent of the *R* chemical state being a consequence of a multielectron

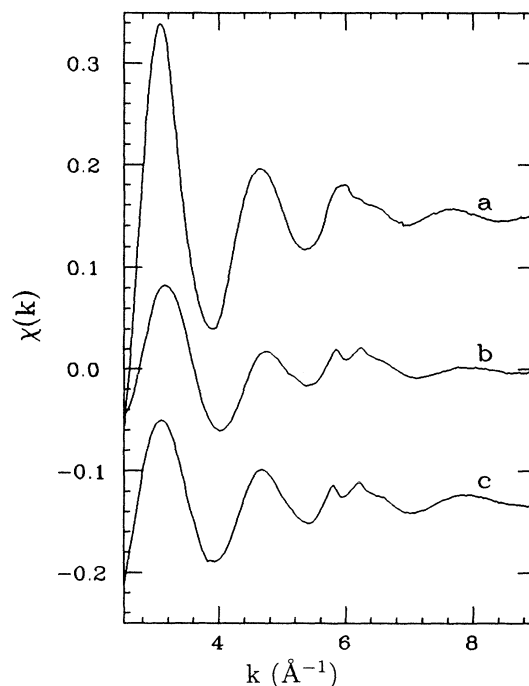


FIG. 12. Comparison of the L_2 , L_3 EXAFS spectra of Ce^{4+} water solution (curves *b* and *c*) with the L_3 EXAFS spectrum of Ce^{3+} (curve *a*). The origin of the vertical axis refers to curve *b*, curves *a* and *c* are shifted downwards and upwards for sake of clarity.

excitation phenomenon. It is worthwhile to note that in this case the anomalous structure is formed by two different peaks which indicate that the two different channels are operating also for the double-electron excitation.^{34,35}

IV. CONCLUSIONS

An extensive x-ray-absorption investigation is presented on *R* water solutions with the aim to characterize the double-electron excitation phenomenon appearing in the EXAFS spectra at the *R L* edges and to study its evolution through the *R* series. This study, together with previous works on some different systems, corroborate the presence of multielectron excitations for these atomic species. We show that the position in energy of the anomalous structures is in agreement with theoretical calculations for the simultaneous transition $2p, 4d \rightarrow 5d, 5d$ in the case of the L_3 and L_2 spectra and $2s, 4d \rightarrow 6p, 5d$ for the L_1 spectra. The intensity of the transition decreases with the rare-earth atomic number, as expected from theory, but the values deduced from the comparison with the main excitation feature are lower than those calculated in Ref. 15 and the anomalous feature is practically absent in the Tm^{3+} spectrum. The origin of these structures is demonstrated to be atomic but a fine structure is ob-

served above the onset energy of the double-electron excitation channel. It could depend on the chemical state of the rare-earth atom suggesting a possible coexistence of atomic and chemical and/or structural effects.

A structural analysis is also reported showing that ionic solutions of rare earths are coordinated by 12 water molecules in a cubooctahedral symmetry, in contrast with previous structural studies of concentrated R^{3+} water solutions.¹⁸⁻²⁰ The presence of the multielectron excitations can distort the EXAFS data analysis leading to errors in the interatomic distances of the order of 0.02 Å, this effect being more important for the low-*Z* rare-earth elements due to the higher intensity of the anomalous structure.

ACKNOWLEDGMENTS

This work has been partially supported by the CICYT Project No. PB1077. The measurements at the Synchrotron Radiation Source of the Daresbury SERC laboratories were carried out within the EEC Large Installations program. The authors thank the Daresbury staff, in particular R. Bilborrow, for the kind assistance during the experiments. The authors also thank J. Chaboy and A. Marcelli for many fruitful discussions.

- ¹H. W. Schnopper, *Phys. Rev.* **131**, 2558 (1963).
²R. P. Madden and K. Codling, *Phys. Rev. Lett.* **10**, 516 (1963).
³U. Fano and J. W. Cooper, *Rev. Mod. Phys.* **40**, 441 (1968).
⁴R. D. Deslattes, R. E. LaVilla, P. L. Cowan, and A. Henins, *Phys. Rev. A* **27**, 923 (1983).
⁵K. Zhang, E. A. Stern, J. J. Rehr, and F. Ellis, *Phys. Rev. B* **44**, 2030 (1991).
⁶P. D'Angelo, A. Di Cicco, A. Filipponi, and N. V. Pavel, *Phys. Rev. B* **47**, 2055 (1993).
⁷A. Filipponi, E. Bernieri, and S. Mobilio, *Phys. Rev. B* **38**, 3298 (1988).
⁸J. Garcia, A. Marcelli, M. Sanchez del Rio, J. Bartolome, D. Fruchart, S. Miraglia, and F. Vaillant, *Physica B* **158**, 521 (1989).
⁹S. Benazeth, M. H. Tuilier, and M. Guittard, *Physica B* **158**, 39 (1989).
¹⁰A. Bianconi, J. Garcia, M. Benfatto, A. Marcelli, C. R. Natoli, and M. F. Ruiz Lopez, *Phys. Rev. B* **43**, 6885 (1991).
¹¹J. Chaboy, J. Garcia, J. Bartolomé, D. Fruchart, S. Miraglia, and A. Marcelli, in *2nd European Conf. on Progress in X-ray Synchrotron Radiation Research*, edited by A. Balerna, E. Bernieri, and S. Mobilio (Compositori, Bologna, 1990), p. 777.
¹²J. Chaboy, J. Garcia, A. Marcelli, and M. F. Ruiz-Lopez, *Chem. Phys. Lett.* **174**, 389 (1990).
¹³J. Purans, A. Kuzmin, and E. Burattini, *Jpn. J. Appl. Phys.* **32**, Suppl. 32-2, 64 (1993).
¹⁴J. Chaboy, J. Garcia, A. Marcelli, and T. A. Tyson, *Jpn. J. Appl. Phys.* **32**, Suppl. 32-2, 61 (1993).
¹⁵J. Chaboy, A. Marcelli, and T. A. Tyson, *Phys. Rev. B* **49**, 11 652 (1994).
¹⁶J. Chaboy and T. A. Tyson, *Phys. Rev. B* **49**, 5869 (1994).
¹⁷G. Materlik, B. Sonntag, and M. Taus, *Phys. Rev. Lett.* **51**, 1300 (1983).
¹⁸M. Benfatto, C. R. Natoli, A. Bianconi, J. Garcia, A. Marcelli, M. Fanfoni, and J. Davoli, *Phys. Rev. B* **34**, 5774 (1986).
¹⁹A. H. Narten and R. L. Hahn, *Science* **217**, 1249 (1982).
²⁰A. Habeschuss and F. H. Spedding, *J. Chem. Phys.* **70**, 3758 (1979).
²¹F. Alan Hart, in *Comprehensive Coordination Chemistry*, edited by G. Wilkinson (Pergamon, Oxford, 1987), Vol. 3, p. 1059.
²²T. K. Sham, in *Topics in Current Chemistry*, edited by M. J. S. Dewar, J. D. Dunitz, K. Hafner, E. Heilbronner, S. Ito, J.-M. Lehn, K. Niedenzu, K. N. Raymond, C. W. Rees, and F. Vögtle (Springer-Verlag, New York, 1988), Vol. 45, p. 81.
²³T. K. Sham, *Phys. Rev. B* **40**, 6045 (1989).
²⁴T. K. Sham, *J. Chem. Phys.* **79**, 1116 (1983).
²⁵See, for example, *X-Ray Absorption: Principles, Applications, Techniques of EXAFS, SEXAFS and XANES*, edited by D. C. Koningsberger and R. Prins (Wiley, New York, 1988).
²⁶J. Chaboy, J. Garcia, and A. Marcelli, *Solid State Commun.* **12**, 939 (1992).
²⁷E. Bernieri and E. Burattini, *Phys. Rev. A* **35**, 3322 (1987).
²⁸J. J. Rehr, J. Mustre de Leon, S. I. Zabinssky, and R. C. Albers, *J. Am. Chem. Soc.* **113**, 5135 (1991).
²⁹D. H. Templeton and C. H. Dauben, *J. Am. Chem. Soc.* **76**, 5237 (1954).
³⁰A. Fert, *Bull. Soc. Franc. Mineral. Crist.* **85**, 267 (1962).
³¹See, Appendix of International Workshop on Standards and Criteria in Absorption X-ray Spectroscopy, Brookhaven National Laboratory, 1988 [*Physica B* **158**, 701 (1989)].
³²A. Kotani, T. Jo, and J. C. Parlebas, *Adv. Phys.* **37**, 37 (1988).
³³J. Rohler, in *Handbook on the Physics and Chemistry of Rare Earths*, edited by K. A. Gschneider Jr., L. Eyring, and S. Hufner (North-Holland, Amsterdam, 1987), Vol. 10, p. 453.
³⁴C. R. Natoli, M. Benfatto, C. Brouder, M. F. Ruiz López, and D. L. Foulis, *Phys. Rev. B* **42**, 1944 (1990).
³⁵E. Beaupaire, J. P. Kappler, D. Malterre, and G. Krill, *Europhys. Lett.* **5**, 369 (1988).